https://doi.org/10.1016/j.chemosphere.2020.127755

Evaluating the Environmental Impact of Contaminated Sediment Column Stabilized by Deep Cement Mixing

Tsz-On Ho [a], Daniel C.W. Tsang [a,*], Wen-Bo Chen [a], and Jian-Hua Yin [a]

[a] Department of Civil and Environmental Engineering, The Hong Kong Polytechnic University, Hung Hom, Kowloon, Hong Kong, China

[*] Corresponding author: dan.tsang@polyu.edu.hk

Abstract

Deep cement mixing (DCM) method is a widely used geotechnical technique for increasing ground stabilization before construction works. However, the environmental influence of stabilized ground on the surrounding area remains a concern. A physical model experiment of DCM-treated sediment column was conducted to investigate both geotechnical and environmental effects on the surrounding sediment. The DCM column contained the cement-stabilized contaminated sediment and surrounded by uncontaminated sediment. The physical behaviour, including settlement, pore water pressure, and total pressure were measured under different loadings. Simultaneously, the migration of the major ions into seawater, and leaching of potentially toxic elements into the surrounding sediment were evaluated. The results revealed that the leaching of major ions from the DCM column followed the dissipation of

excess pore water and migrated to the seawater above the sediment surface. Nevertheless, the leaching behaviour of potentially toxic elements into the surrounding sediment and variation of pH value after the DCM treatment were within an acceptable level. Therefore, the contaminated marine sediment could be effectively stabilized and solidified by *in-situ* remediation with minimal secondary pollution to the surrounding environment.

Keywords: contaminated sediment; *in-situ* remediation; stabilization/solidification; long-term consolidation; metal/metalloid leaching; environmental pollution.

Introduction

Due to the increasing demand of the land for urban development and metropolitan area, it is difficult to find an appropriate ground in densely populated cities such as Hong Kong. Reclamation on marine sediment, which is often contaminated, is an effective way to solve this problem, which has been adopted in the third runway establishment of the Hong Kong International Airport (HKIA). In the reclamation, the soft and contaminated sediment requires proper *in-situ* improvement techniques to minimize the contaminant leaching, increase the mechanical strength, and reduce the long-term settlement. Among commercially available techniques, deep cement mixing (DCM) method is considered as the most effective technique (Yin, 2001). This method has been developed and widely used in Japan and Nordic countries

(Kitazume and Terashi, 2013; Long *et al.,* 2019) because the strength of the stabilized/solidified (S/S) sediment can be significantly increased within a short period of time compare other ground improvement techniques (Chiu *et al*., 2019; Li *et al.,* 2019; Reddy *et al*., 2019; Wang et al., 2019a; Xia *et al.,* 2019). In addition, the contaminated marine sediment can be simultaneously remediated by mixing with binders such as cement, lime, or lime-base materials. (Wang *et al.,* 2015b; Li *et al .,* 2017; Wang *et al.,* 2020b).

Marine Sediment contamination is a global problem (Birch, 2017; Niu *et al.,* 2020; Wang *et al.,* 2020a). Due to the historical pollution by industrial and domestic sewage discharges, various levels of potentially toxic elements (PTEs) in the marine sediments were found in many regions across Hong Kong (HK EPD, 2013). The dredged sediments were classified based on the level of pollution, and the contaminated sediments were dumped in the designated open sea disposal areas or contaminated mud pits (CMPs) depending on the contamination levels, and continuous monitoring program was required (HK ETWB 2002). To reduce the environmental impacts of dredged/excavated sediment, non-dredging *in-situ* reclamation method of former CMPs marine area is needed for reclamation and future development, which is an imperative and cross-disciplinary challenge to geotechnical and environmental researchers. Recent studies have advanced the *ex-situ* S/S technique for recycling of the contaminated sediment into sediment-based products including non-load-bearing blocks (Wang *et al.,* 2015), high-strength

pedestrian blocks (Wang *et al.,* 2017), and eco-paving blocks (Wang *et al.*, 2018a). Economic applicability of different sediment-derived blocks showed further support for the development of novel and sustainable management of contaminated sediment (Wang *et al.,* 2018b). *In-situ* and *ex-situ* S/S treatment of hazardous materials became mature after appropriate curing methods (Cui and Jing, 2019; Wang *et al.,* 2019b; Wang *et al.,* 2019c) and presented low risk in the long-term performance (Gomes *et al*., 2019; Oustriere *et al.,* 2016; Shen *et al.,* 2018), therefore the S/S technique is widely accepted and utilized.

DCM method can be considered as an *in-situ* S/S process which can stabilize the contaminated sediment under the water column (i.e., without prior dredging) and minimize the marine environmental impacts during and after the construction process (Wang *et al.,* 2014a; Libralato *et al.,* 2018; Ma *et al.,* 2020). It has become popular in various projects, e.g., such as reclamation for Tung Chung New Town Extension and the third-runway system projects in Hong Kong. Most of the previous studies focused on mechanical and transport properties of the soft sediment treated by DCM, such as strength, stiffness, and permeability (He *et al.,* 2018; Gomes et al., 2020; Horpibulsuk *et al.,*2005; Quang and Chai, 2015; Yin, 2004). For example, Yin and Fang (2006) prepared a small-scale experiment and evaluated the relative permeability of the DCM with regard to the surrounding sediment, which suggested that the DCM column could be regarded as a partial or full vertical drainage. Fang and Yin (2007) investigated the

75 dissipation of excess pore water pressure and development of stress concentration in a
76 composite foundation under multi-staged loading revealed that the presence of DCM column
77 increased the speed of dissipation of excess pore water pressure in the composited foundation.
78 Horpibulsuk *et al.* (2012) revealed that the rates of dissipation of excess pore water pressure in
79 both DCM column and the surrounding environment were almost the same at different depths
80 of the composite ground. DCM columns are known to establish their setting and gain strength
81 through chemical reactions, including hydration of binders, ion exchange reaction, and
82 formation of cement hydration products and pozzolanic reaction products (Kitazume and
83 Terashi, 2013). CaO as the major ingredient of cement reacts with water and produces calcium
84 (Ca^{2+}) and hydroxide (OH^{-}) that may migrate into the surrounding environment in the curing
85 period (Larsson *et al*., 2009). Ikegami *et al.* (2005) indicated that the Ca^{2+} leaching from treated
86 soil was one of the major factors that caused the deterioration of the circumstantial environment
87 and ecological system, as a result of the concentration gradient between DCM column and
88 surrounding area. In particular, the time-dependent performance and effectiveness for the
89 environmental risk mitigation remain a concern (Rađenović *et al*., 2019; Xia *et al*., 2019).
90 There is a legitimate need to understand the change of physicochemical properties of DCM
91 column and the surrounding environment.
92
93 There is a knowledge gap in the existing literature regarding the coupling of consolidation

94 behaviour and the extent of ion migration into the surrounding environment after the *in-situ*
95 sediment remediation using DCM column technology, which may lead to the second pollution
96 risk. In this study, an axisymmetric physical model test was designed and conducted to
97 particularly assess the ion migration between the DCM column and surrounding sediment.
98 Sediment and pore water samples at different radial distances and different depths were
99 analyzed during the DCM column consolidation. The pH values and chemical concentrations
100 were monitored for understanding the migration mechanism of major cations and PTEs in the
101 *in-situ* sediment remediation process. The results in this study can serve as a reference for better
102 understanding of the environmental issue in reclamation design.
103

104 # Experimental Methods

105 ## Materials

106 *Hong Kong Marine Sediment (HKMS) and Contaminated Hong Kong Marine Sediment*
107 *(CHKMS)*

108 The HKMS used in this study was obtained from Lantau Island in Hong Kong. The total metal
109 concentrations in the HKMS were 16 mg/kg of Cu, 71 mg/kg of Zn, 36 mg/kg of Cr, 21 mg/kg
110 of Ni, and 6 mg/kg of As. The CHKMS was taken from the deep seabed about 5 m underwater
111 in the CMPs to the South of Brothers in Hong Kong. The total metal concentrations in the

CHKMS were 15 mg/kg of Cu, 87 mg/kg of Zn, 38 mg/kg of Cr, 23 mg/kg of Ni, and 9.5 mg/kg of As. The physical properties and total metal concentrations of HKMS and CHKMS are listed in Tables 1 and 2.

Cement material

The cement used in the test to form the DCM column is Type I Ordinary Portland Cement (OPC) locally produced by Green Island group, Hong Kong. To ensure a consistent composition, the cement from the same batch of production was used. The chemical composition of the cement used in this study is shown in Table 3.

Physical Model Test

A cylindrical stainless-steel mould of 300 mm in inner diameter and 400 mm in height was used for the experimental study. The physical model was built to simulate the unit element of the HKMS improved by a DCM column. The DCM column was surrounded by the pre-consolidated HKMS. A rigid plate was put on the top of the model applying the vertical displacement for both DCM column and HKMS. The lateral displacement is not permitted. The vertical load was applied by a pneumatic jack system, which could maintain a stable loading. The detailed arrangement of the equipment is shown in Fig. 1.

130

131 *Sediment Preparation*

132 HKMS used in this study was firstly mixed with a specified quantity of seawater thoroughly
133 by a motorized mixer with a water content of 1.9 times the liquid limit of the clayey sediment
134 (*i.e.* 102% water content) (Yin and Fang 2010). Then the HKMS slurry was reconstituted in
135 the cylindrical model and was pre-consolidated uniaxially under 15 kPa by dead weights. To
136 accelerate the consolidation process, the drainages from the top and bottom surfaces were
137 allowed in the pre-consolidation stage. The initial height of slurry was estimated to be 350 mm.
138 The final height of the HKMS after pre-consolidation was about 280 mm. The pre-
139 consolidation stage lasted for 33 days, and the measured excess pore water pressure is less than
140 1 kPa. The height of HKMS was trimmed to 230 mm as a designed height, and a sampling port
141 with a diameter of 50 mm was drilled for inserting a DCM column.

142

143 *DCM Column Formation and Curing*

144 Since the physical model simulated a marine ground improvement technique, seawater was
145 used to prepare the DCM columns (instead of distilled water) to reduce experimental
146 discrepancy from the field conditions (Li et al., 2020) The initial water content of CHKMS was
147 35%. The CHKMS was mixed with additional seawater reaching the state with a water content

148 of 100%. The cement content was kept at 25%, which was defined as the ratio of the dry mass
149 of cement to that of sediment. The dry cement powder was added and mixed thoroughly by an
150 electric mixer for 5 mins.
151
152 Then the mixture was placed into a PVC tube mould with an internal diameter of 50 mm and a
153 height of 200 mm. The paste was compacted in three layers that each layer was tamped with a
154 hammer for ten times. After curing for one day inside the PVC mould, the DCM column was
155 transferred into the pre-drilled hole in the pre-consolidated HKMS. The DCM column was
156 cured in the composite foundation model.
157
158 After inserting the DCM column, a 50 mm sand layer was placed to cover both the HKMS and
159 DCM column. The curing time was 52 days. The preparation aimed to obtain a uniform DCM
160 column and ensure that curing condition under clay environment was close to the real project.
161
162 *Instrumentation*
163 In this physical model, five pore water pressures transducers (PPTs) were used to measure the
164 variations of pore water pressure inside the HKMS. The PPTs are 18 mm in diameter and 13
165 mm in thickness with a capacity of 200 kPa. Two earth pressure cells (EPCs) were used to

166 measure the loads acting on the DCM column and the HKMS, respectively. The EPCs are 28
167 mm in diameter and 10 mm in thickness. The EPCs and PPTs were carefully calibrated before
168 the physical testing, and details could be referred to Feng *et al.* (2016) and Qin *et al.* (2019).
169 Two linear variable differential transformers (LVDTs) were used to measure the settlement of
170 the composite ground. Loading was applied by a pneumatic jack system which provides
171 different vertical loadings to the physical model by adjusting the air pressure. A 30-kN capacity
172 loading cell was used for measuring the applied loading on the model. All the transducers were
173 connected to the data logger (NI PXIe-1082, National Instruments) for collecting continuous
174 data.
175

176 *Loading and Sampling Procedures*

177 After curing, a rigid plate was placed on the top of the sand layer. The multistage loading (15
178 kPa, 20 kPa, 40 kPa, and 60 kPa) was applied by steps. Under each stage of loading, the top of
179 the model was drained while the bottom valve was closed to simulate the actual drainage. The
180 loading and sampling schedule are plotted in Fig. 2
181

182 Sediment samples were collected in each stage after the consolidation completed. There was a
183 4-sampling port system (*i.e.,* 16 sampling positions) on the physical model tank, as shown in

184 Fig. 1, with each entrance point connecting a valve. Each set included four sampling ports with
185 50-mm interval (30 mm, 80 mm 130 mm and 180 mm from the bottom of the DCM column).
186 During sampling, the entrance valve was open, and the sediment was sampled by inserting a
187 125 mm length and 8 mm diameter sampling tube horizontally into the model as shown in Fig.
188 3a-c. This method could retrieve about 2 g of dry clay beam in each slot. The advantage of this
189 method was that vertical loads could be continuously applied to the system, thereby reducing
190 the interference of the consolidation process of the composition foundation. Four sediment
191 samples were extracted from the model as shown in Fig. 3. All clay samples were oven-dried
192 at 105°C for 24 h.
193

194 *Chemical Properties*

195 Chemical properties determined in this study include pH value of the seawater on the top of
196 the HKMS, major cations and PTEs concentration of the surrounding HKMS and seawater.
197 The pH values of surface seawater were measured by a portable pH meter. The pH values were
198 measured at the centre and two edges (left side and right side) of the top of the surface seawater
199 on the model experiments every time.
200

201 Sediment samples were prepared according to the following total digestion procedures. Each

oven-dried sediment sample was cut into three pieces as shown in Fig. 3d. A 0.25 g of ground sediment sample was heat digested with a mixture of concentrated nitric acid (HNO_3) and perchloric acid ($HClO_4$) on a hot block with a ratio of 4:1. After cooling down, 10 mL of 5% HNO_3 was added into the slurry, and the slurry was filtered by the 0.45 μm microfiltration membrane. The solutions were quantified by Inductively Coupled Plasma-Optical Emission Spectroscopy (ICP-OES) determination of cations and PTEs concentrations.

For the sampled seawater, 5 mL of the water sample was mixed with 2 mL concentrated nitric acid (HNO_3) and digested. After cooling down to room temperature, 5 mL of 5% HNO_3 was mixed with specimens. The mixture was filtered by the 0.45 μm microfiltration membrane and the concentrations of major cations and PTEs were determined by the ICP-OES analysis.

Results and Discussion

Seawater pH Value

During the loading stage, the consolidation process only allowed pore water to drain from the top surface of the physical model. The initial pH value of seawater was 7.86. Fig. 4 shows the change of pH value of seawater with time under increasing loading. The pH values of the seawater were measured at the centre and two sides of the model. The pH value raised from

7.86 to a peak of 8.4 under 15 kPa loading. The maximum pH values were 8.4 and 8.3 under 20 kPa and 40 kPa, respectively. After the mechanical failure of the column, there was no increase in pH value even though the loading increases to 60 kPa, pH value remained stable at 8.1.

The increase of pH value after each loading could be attributed to the dissipation of excess pore water pressure, which would induce the drainage of water from the surrounding sediment to the top surface. Besides, there was a certain delay for the increase in pH value after each loading step, probably because of the low permeability of the HKMS such that the pore water took longer time to drain to the top surface. The pH value in each loading step fell to a stable level after reaching a peak value. This was probably due to the carbonation by CO_2 from the atmosphere and its attainment of equilibrium condition (Wang et al., 2014a; Wang et al., 2014b). Setunge et al. (2009) observed similar phenomenon and pointed out that the pH value was influenced by the dosage of cement content because the pH value could be influenced by the leaching of calcium hydroxide. On the other hand, the increase of cement dosage reduced the porosity of DCM column, which could mitigate the leaching behaviour and delay the increase in pH value, accounting for the small fluctuation of pH after a long time of loading. It can be concluded that the variations of pH value due to DCM column were considered environmentally acceptable in the marine environment.

Stresses on DCM Column and the Surrounding Sediment

The settlement of the composite foundation is shown in Fig. 2. The total final settlement was 40 mm, and the loading period was 122 days. The DCM column failed under the loading of 40 kPa, and then the settlement increased quickly. There was a slight influence of sediment sampling on the settlement. Fig. 5 shows the total stresses on the DCM column and surrounding sediment versus time with the stress concentration ratio n under four loading stages. The stress concentration ratio, *n*, was defined as the ratio of total stress on the column to that on the surrounding ground, which is an important parameter to analyze the loading distribution in the column-treated sediment. However, many factors were affecting the stress concentration ratio, for example, the consolidation degree of the surrounding sediment, the magnitude of the loading, condition of loading, and the dimension and stiffness of the DCM column, *etc.* (Fang and Yin, 2007). There were two different loading conditions which are flexible and rigid loading. Stresses on DCM column and surrounding sediment were uniform if the loading was flexible and the parameter n was a constant. In this physical model, the loading was considered as a rigid loading as a rigid plate was placed on the top. Fig. 5 shows that the *n* value varies with vertical loading, and it was not a constant value. In the first two loading stages, *i.e.* 15 kPa and 20 kPa loadings, the *n* value increased when the applied load increased. This indicates that the stress was transferred from sediment to column until force equilibrium. A similar

conclusion was drawn on the increasing n value with time before the failure of column (Yin and Fang, 2006). They found that local crushing occurred upon the failure of column, after which n value decreased with time. A similar phenomenon is shown in Fig. 5b, when applying 40 kPa loading on the composite ground, the failure of column occurred and the n value displayed a sudden drop. The stress on the DCM column decreased with time when the applied load was increased to 60 kPa, as shown in Fig 5a. The loading started to transfer back from the DCM column to the surrounding sediment. Therefore, the *n* value kept decreasing.

Leaching Behaviour of Major Cations and PTEs in Seawater

During the cement hydration reaction, certain amounts of cations, Ca^{2+}, Mg^{2+}, Fe^{3+} were dissolved into the pore water from the DCM column. There were higher concentrations of major cations in the pore water and the surrounding sediment. The concentrations of major cations Mg^{2+}, Ca^{2+}, K^{+} and Al^{3+} were measured. After the curing stage, the first loading 15 kPa was added, and the concentration of Mg^{2+} increased as shown in Fig. 6a. The concentration of Mg^{2+} kept rising when the loading increased from 790 mg/L to the maximum value of 980 mg/L at 40 kPa loading, and it stabilized at about 950 mg/L. There was a similar phenomenon occurring on K^{+}. The continuous growth of the concentrations was observed in the loading stages from about 350 mg/L to 400 mg/L. However, the concentration of Ca^{2+} increased rapidly

275 at 15 kPa loading stage from 370 mg/L to the maximum value of 460 mg/L as shown in Fig.
276 6c. Unlike Mg^{2+} and K^{+}, the concentration of Ca^{2+} remained relatively stable at 390 mg/L even
277 though the applied loading further increased. In contrast, the concentration of Al^{3+} maintained
278 at a stable value at 0.55 mg/L in the seawater.
279
280 It is shown that the concentrations of monovalent cation K^{+} increased during the loading stage,
281 although K^{+} was not present in the cement used. This probably resulted from cation exchange
282 because trivalent and divalent cations would have the ability to replace the monovalent cations
283 (Shen et al., 2008). After installation of the DCM column, pore seawater showed higher
284 concentrations of divalent cations such as Ca^{2+} than monovalent cations. The monovalent
285 cations such as K^{+} that were initially adsorbed on the surface of surrounding sediment were
286 replaced by the divalent cations diffusing out from the DCM column. As the concentration of
287 trivalent Al^{3+} was low, the ion exchange effect was not significant. During the loading stage,
288 the excess pore water was dissipated to the ground surface, the concentration of K^{+} in the
289 seawater increased accordingly. Fig. 6b shows that cation concentrations increased even before
290 the failure of the DCM column. However, more micro-cracks might be induced during the
291 increase of loading before the DCM column failure. The increasing concentrations of major
292 cations may be ascribed to the continuous increase in the number of micro-cracks in the DCM
293 column.

294

295 All the PTEs concentrations in the CHKMS were below the hazardous level according to the
296 management guidelines in Hong Kong (HK ETWB 2002). The trends of leaching behaviour of
297 some PTEs into seawater could be observed, although most of the results were below 1 mg/L.
298 The concentrations of As, Zn, Cu, Mn, Ni, and Cr showed a rising trend. The concentration of
299 Zn showed a noticeable increase from 0.076 mg/L to a maximum value of 0.136 mg/L after 15
300 kPa loading, then reduced to a stable value of 0.107 mg/L as shown in Fig. 7. A similar result
301 was obtained for Cu, the concentration of which increased from 0.035 mg/L to a maximum
302 value of 0.065 mg/L at 15 kPa loading. When loading was further increased to 40 kPa, its
303 concentration remained stable at 0.050 mg/L. Similarly, the concentration of Mn increased
304 from 0.049 mg/L to 1.856 mg/L, and the concentration of Ni increased from 0.143 mg/L to 0.9
305 mg/L. Only the concentration of Cr remained stable at 0.09 mg/L under all loadings even after
306 the DCM column failure. The concentration of As in the seawater was less than 0.001 mg/L
307 throughout the process.

308

309 *Leaching Behaviour of Major Cations and PTEs in the Surrounding Sediment*

310 In order to understand the leaching behaviour after the DCM column-treated remediation,
311 sediment samples were collected from the physical model experiment under different depths

312 and loadings. Fig. 8a shows that the distribution of concentration of Mg^{2+} with different depths
313 and horizontal distances away from the DCM column in the physical model under various
314 loadings. At the locations with distances of 0 to 40 mm from the edge of the DCM column, the
315 concentration of Mg^{2+} increased with increasing loading. This trend could be observed at the
316 sampling port 4 from 9.5 g/kg to 12.5 g/kg. The concentration of Mg^{2+} became relatively stable
317 at approximately 9 g/kg in the surrounding sediment located 42 to 125 mm away from the
318 DCM column. The samples from the sampling ports 2 and 3 displayed the same phenomenon.
319 Similar changes were displayed by Ca^{2+} as shown in Fig. 8b. The samples from the sampling
320 ports 2, 3 and 4 showed an increasing concentration of Ca^{2+} under increment loading location
321 0 – 42 mm from the DCM column. The highest concentration of the point near to DCM column
322 occurred when 40 kPa loading was applied. It rose from 12.5 g/kg (before loading) to 16 g/kg.
323 This suggests that the ion migration was predominantly driven by the upward dissipation of
324 excess pore water and at the same time the ion diffusion into the surrounding sediment. There
325 might be some vertical fractures developed in the surrounding sediment during the installation
326 of DCM columns, which could provide a drainage boundary for excess pore water to diffuse
327 from the ground to the surface water (Shen *et al.,* 2008).
328
329 The effect of applied vertical loading was observed on PTEs leaching into the surrounding
330 sediment. In the location ranging from 0 to 42 mm, the concentration of As showed a slight

increase when the vertical loading increased (Fig. 8c). When the distance from the DCM column increased (i.e., 42 – 125 mm from the column), the concentration of As at the same location under different loading levels showed a similar trend. In comparison, the other concentrations of PTEs (Zn, Cu, Mn, Ni, and Cr) were steady, and the increment concentration of each PTE was less than 10% compared with the initial value. The results suggest that DCM column-treated sediment could effectively stabilize the PTEs elements.

Pore Water Pressure in the Stabilized/Solidified Sediment

During the loading stage, the drainage was only permitted through the top surface. Under each loading stage, excess pore water pressure was induced. The pore water pressure firstly increased to the maximum value and then started to dissipate. Fig. 9 shows that the pore water pressure changed with time under 15 kPa by comparing three sensors (PPT 1, PPT 2, and PPT 4) at the same height level. When the 15 kPa was applied, PPT 4 manifested the maximum pore water pressure of 6 kPa near to the DCM column. When the distance from the column increased, the maximum pore water pressures increased to 8 kPa (PPT 2) and 9 kPa (PPT 1). This is possibly because the DCM column sustained the majority of the force, then the surrounding sediment was subjected to a lower pressure such that the peak value was also lower. Since there was a pressure difference between the outer periphery and inner core of the S/S sediment, the

dispersion of excess water pressure can be considered as flowing horizontally from the DCM column to the surrounding environment. It may explain why the ion concentrations in the pore water kept increasing. Fig. 9 indicates that the degree of consolidation of the sediment adjacent to the DCM column was lower than that far away from the column. After applying the loading for eight days, the degree of consolidation could reach 98% in the surrounding sediment and 85% for the sediment close to the DCM column. The excess pore water pressure changed with time in a similar way under the loadings of 20 kPa (Fig.S1), 40 kPa (Fig.S2), and 60 kPa (Fig.S3), respectively.

Conclusions

A physical model experiment was conducted to evaluate the physicochemical properties of the DCM-treated contaminated sediment column and the surrounding sediment under multi-staged loading. It was observed that the seawater pH value varied with the staged loading. The concentrations of major cations increased and migrated into the seawater due to the dissipation of pore water, possibly because of fractures caused by the installation of DCM column and micro-cracks induced by the continuous loading. The concentrations of PTEs in the surrounding seawater were found to be stable even under an increasing loading. There were minimal amounts of major cations and PTEs diffusion into the surrounding sediment. The

physical model experiments showed that the ion migration to the surrounding environment was mainly attributed to the consolidation behaviour and the upward flow of the seawater during the dissipation of pore water pressure. Therefore, the risk of secondary pollution to the surrounding environment was considered low when using the DCM ground improvement, even with the failure of DCM columns under high pressures. This study confirmed that the marine sediment of low contamination level could be effectively stabilized and solidified for the land reclamation by using the *in situ* DCM method. Further research will be required for evaluating the treatment effectiveness for heavily contaminated sediment.

Acknowledgments

This study was supported by Research Impact Fund (RIF) project (R5037-18), Theme-based Research Scheme Fund (TRS) project (T22-502/18-R), and General Research Fund (GRF) projects (PolyU 152796/16E, PolyU 152209/17E; PolyU 152179/18E) from Research Grants Council (RGC) of Hong Kong Special Administrative Region Government of China. The authors also acknowledge the financial support from the Research Institute for Sustainable Urban Development and The Hong Kong Polytechnic University (BBAG, ZDBS, ZVNC).

References

Birch, G.F., 2017. Determination of sediment metal background concentrations and enrichment in marine environments - a critical review. Sci. Total Environ. 580, 813–831. https://doi.org/10.1016/j.scitotenv.2016.12.028.

Chiu, A. C., Akesseh, R., Moumouni, I. M., Xiao, Y. 2019. Laboratory assessment of rice husk ash (RHA) in the solidification/stabilization of heavy metal contaminated slurry. J. Hazard Mater.371, 62-71. https://doi.org/10.1016/j.jhazmat.2019.02.051.

Cui, J., Jing, C., 2019. A review of arsenic interfacial geochemistry in groundwater and the role of organic matter. Ecotox. Environ. Safe.183, 109550. https://doi.org/10.1016/j.ecoenv.2019.109550.

Gomes, S. D. C., Zhou, J. L., Li, W., Long, G., 2019. Progress in manufacture and properties of construction materials incorporating water treatment sludge: A review. Recour. Consery. Recy. 145, 148-159. https://doi.org/10.1016/j.resconrec.2019.02.032

Gomes, S. D. C., Zhou, J. L., Li, W., Qu, F. 2020. Recycling of raw water treatment sludge in cementitious composites: effects on heat evolution, compressive strength and microstructure. Recour. Consery. Recy. 161, 104970. https://doi.org/10.1016/j.resconrec.2020.104970.

HK EPD, 2013. Marine Water Quality in Hong Kong in 2012. Environmental Protection Department, Hong Kong SAR Government.

HK ETWB, 2002. Management of dredged/excavated sediment. Appendix A of ETWB (W) No, 34, A1. Environment, Transport and Works Bureau, Hong Kong SAR Government.

Fang, Z., Yin, J.H., 2007. Responses of excess pore water pressure in soft marine clay around a soil–cement column. Int. J. Geomech. *7*(3), 167-175. https://doi.org/10.1061/(ASCE)1532-3641(2007)7:3(167).

Feng, W.Q., Liu, Z.Y., Tam, H.Y., Yin, J.H., 2016. The pore water pressure sensor based on Sagnac interferometer with polarization-maintaining photonic crystal fiber for the geotechnical engineering. Measurement, 90, 208-214. https://doi.org/10.1016/j.measurement.2016.04.067.

He, Y., Yang, H., Yang, J., Liu, H., Zhao, P., 2018. Research on Laboratory Mixing Trial of

Marine Deposit and Cement in Hong Kong. *Paper presented at the* GeoShanghai International Conference. https://doi.org/10.1007/978-981-13-0122-3_25.

Horpibulsuk, S., Chinkulkijniwat, A., Cholphatsorn, A., Suebsuk, J., Liu, M. D., 2012. Consolidation behavior of soil–cement column improved ground. Comput. Geotech. *43*, 37-50. https://doi.org/10.1016/j.compgeo.2012.02.003.

Horpibulsuk, S., Miura, N., Nagaraj, T., 2005. Clay–water⁄ cement ratio identity for cement admixed soft clays. J. Geotech. Geoenviron.*131*(2), 187-192. https://doi.org/10.1061/(ASCE)1090-0241(2005)131:2(187).

Kitazume, M., Terashi, M., 2013. The deep mixing method. CRC press.

Larsson, S., Rothhämel, M., Jacks, G., 2009. A laboratory study on strength loss in kaolin surrounding lime–cement columns. Appl. Clay Sci. 44(1-2), 116-126. https://doi.org/10.1016/j.clay.2008.12.009.

Libralato, G., Minetto, D., Lofrano, G., Guida, M., Carotenuto, M., Aliberti, F., Conte, B., Notarnicola, M., 2018. Toxicity assessment within the application of in situ contaminated sediment remediation technologies: A review. Sci. Total Environ. 621, 85-94. https://doi.org/10.1016/j.scitotenv.2017.11.229.

Li, J. S., Beiyuan, J., Tsang, D. C., Wang, L., Poon, C. S., Li, X. D., Fendorf, S., 2017. Arsenic-containing soil from geogenic source in Hong Kong: leaching characteristics and stabilization/solidification. *Chemosphere*. 182, 31-39. https://doi.org/10.1016/j.chemosphere.2017.05.019.

Li, P., Li, W., Yu, T., Qu, F., Tam, V. W.,2020. Investigation on early-age hydration, mechanical properties and microstructure of seawater sea sand cement mortar. Constr. Build Mater. 249, 118776.

Li, W., Ni, P., Yi, Y., 2019. Comparison of reactive magnesia, quick lime, and ordinary Portland cement for stabilization/solidification of heavy metal-contaminated soils. Sci. Total

438 Environ. 671, 741-753. https://doi.org/10.1016/j.scitotenv.2019.03.270.
439 Long, G., Li, L., Li, W., Ma, K., Dong, W., Bai, C., Zhou, J. L. 2019. Enhanced mechanical
440 properties and durability of coal gangue reinforced cement-soil mixture for foundation
441 treatments. J. Clean Prod. 231, 468-482. https://doi.org/10.1016/j.jclepro.2019.05.210.
442 Ma, B., Wang, Z., Yuan, X., Cen, K., Li, J., Yang, N., Zhu, X., 2020. In situ stabilization of
443 heavy metals in a tailing pond with a new method for the addition of mineral stabilizers—
444 high-pressure rotary jet technology. Environ. Sci. Pollut R. 1-13.
445 https://doi.org/10.1007/s11356-020-07782-9.
446 Mitchell, J., 1993. Fundamentals of Soil Behaviour. In: Wiley, New York.
447 Niu, Y., Jiang, X., Wang, K., Xia, J., Jiao, W., Niu, Y., Yu, H., 2020. Meta analysis of heavy
448 metal pollution and sources in surface sediments of Lake Taihu, China. Sci. Total Environ.
449 700, 134509. https://doi.org/10.1016/j.scitotenv.2019.134509.
450 Oustriere, N., Marchand, L., Lottier, N., Motelica, M., Mench, M., 2017. Long-term Cu
451 stabilization and biomass yields of Giant reed and poplar after adding a biochar, alone or
452 with iron grit, into a contaminated soil from a wood preservation site. Sci. Total Environ.
453 579, 620-627. https://doi.org/10.1016/j.scitotenv.2016.11.048.
454 Qin, J. Q., Feng, W. Q., Wu, P. C., Yin, J. H. 2020. Fabrication and performance evaluation of
455 a novel FBG-based effective stress cell for directly measuring effective stress in saturated
456 soils. *Measurement*, 155, 107491. https://doi.org/10.1016/j.measurement.2020.107491.
457 Quang, N. D., Chai, J. C., 2015. Permeability of lime-and cement-treated clayey soils. Can.
458 Geotech. J. *52*(9), 1221-1227. https://doi.org/10.1139/cgj-2014-0134.
459 Rađenović, D., Kerkez, Đ., Pilipović, D. T., Dubovina, M., Grba, N., Krčmar, D., Dalmacija,
460 B., 2019. Long-term application of stabilization/solidification technique on highly
461 contaminated sediments with environment risk assessment. Sci. Total Environ. 684, 186-
462 195. https://doi.org/10.1016/j.scitotenv.2019.05.351.

463 Reddy, V. A., Solanki, C. H., Kumar, S., Reddy, K. R., Du, Y. J., 2019. New ternary blend
464 limestone calcined clay cement for solidification/stabilization of zinc contaminated soil.
465 *Chemosphere*. 235, 308-315. https://doi.org/10.1016/j.chemosphere.2019.06.051.
466 Setunge, S., Nguyen, N., Alexander, B. L., Dutton, L., 2009. Leaching of alkali from concrete
467 in contact with waterways. Water Air Soil Poll., 9, 381.
468 Shen, Z., Hou, D., Xu, W., Zhang, J., Jin, F., Zhao, B., Pan, S., Peng, T., Alessi, D. S., 2018.
469 Assessing long-term stability of cadmium and lead in a soil washing residue amended with
470 MgO-based binders using quantitative accelerated ageing. Sci. Total Environ. 643, 1571-
471 1578. https://doi.org/10.1016/j.scitotenv.2018.06.321.
472 Shen,S.L.,Han,J.,Du,Y. J., 2008. Deep mixing induced property changes in surrounding
473 sensitive marine clays. J. Geotech. Geoenviron. 134, 845-854. 10.1061/(ASCE)1090-
474 0241(2008)134:6(845).
475 Wang, F., Al-Tabbaa, A. 2014a. Leachability of 17-Year-Old Stabilized/Solidified
476 Contaminated Site Soils. In Geo-Congress 2014: Geo-characterization and Modeling for
477 Sustainability. 1612-1624. https://doi.org/10.1061/9780784413272.158.
478 Wang, F., Wang, H., Al-Tabbaa, A. 2014b. Leachability and heavy metal speciation of 17-year
479 old stabilized/solidified contaminated site soils. J. Hazard Mater. 278, 144-151.
480 https://doi.org/10.1016/j.jhazmat.2014.05.102.
481 Wang, F., Shen, Z., Liu, R., Zhang, Y., Xu, J., Al-Tabbaa, A. 2020. GMCs stabilized/solidified
482 Pb/Zn contaminated soil under different curing temperature: Physical and microstructural
483 properties. Chemosphere. 239, 124738.
484 https://doi.org/10.1016/j.chemosphere.2019.124738.
485 Wang, F., Wang, H., Al-Tabbaa, A., 2015. Time-dependent performance of soil mix technology
486 stabilized/solidified contaminated site soil. J. Hazard Mater. 286, 503-508.
487 https://doi.org/10.1016/j.jhazmat.2015.01.007.

Wang, L., Chen, L., Tsang, D.C.W, Li, J.S., Yeung, T.L., Ding, S., Poon, C.S., 2018a. Green remediation of contaminated sediment by stabilization/solidification with industrial by-products and CO_2 utilization. Sci. Total Environ. *631*, 1321-1327. https://doi.org/10.1016/j.scitotenv.2018.03.103.

Wang, L., Chen, L., Tsang, D.C.W, Li, J.S., Baek, K., Hou, D., Poon, C.S., 2018b. Recycling dredged sediment into fill materials, partition blocks, and paving blocks: Technical and economic assessment. J. Clean Prod. *199*, 69-76. https://doi.org/10.1016/j.jclepro.2018.07.165.

Wang, L., Tsang, D.C.W, & Poon, C.S., 2015. Green remediation and recycling of contaminated sediment by waste-incorporated stabilization/solidification. *Chemosphere.* *122*, 257-264. https://doi.org/10.1016/j.chemosphere.2014.11.071.

Wang, L., Chen, L., Cho, D.W., Tsang, D.C.W., Yang, J., Hou, D.Y., Baek, K., Kua, H.W., Poon, C.S. 2019a. Novel synergy of Si-rich minerals and reactive MgO for stabilization/solidification of contaminated sediment. J. Hazard Mater. 365, 695-706. https://doi.org/10.1016/j.jhazmat.2018.11.067.

Wang, L., Tsang, D.C.W, Zhou, Y.Y., Rinklebe, J., Song, H., Kown, E.E., Baek, K., Ok, Y.S., 2019b. Mechanistic insights into red mud, blast furnace slag, or metakaolin-assisted stabilization/solidification of arsenic-contaminated sediment. Environ. Int. 133, 105247. https://doi.org/10.1016/j.envint.2019.105247.

Wang, L., Chen, L., Tsang, D.C.W., Kua, H.W., Yang, J., Ok, Y.S., Ding, S.M., Hou, D.Y., Poon, C.S., 2019c. The roles of biochar as green admixture for sediment-based construction products. Cement Concrete Comp. 104, 103348. https://doi.org/10.1016/j.cemconcomp.2019.103348.

Wang, L., Yeung, T. L., Lau, A. Y., Tsang, D.C.W, Poon, C.S., 2017. Recycling contaminated sediment into eco-friendly paving blocks by a combination of binary cement and carbon

513 dioxide curing. J. Clean Prod. 164, 1279-1288.
514 https://doi.org/10.1016/j.jclepro.2017.07.070.
515 Wang, L., Chen, L., Guo, B., Tsang, D.C.W., Huang, L., Ok, Y.S., Mechtcherine, V. 2020. Red
516 mud-enhanced magnesium phosphate cement for remediation of Pb and As contaminated
517 soil. J. Hazard Mater. 400, 123317. https://doi.org/10.1016/j.jhazmat.2020.123317.
518 Wang, X., Fu, R., Li, H., Zhang, Y., Lu, M., Xiao, K., Zhang, X., Zheng C., Xiong, Y. 2020b.
519 Heavy metal contamination in surface sediments: A comprehensive, large-scale evaluation
520 for the Bohai Sea, China. Environ. Pollut. 260, 113986.
521 https://doi.org/10.1016/j.envpol.2020.113986.
522 Xia, M., Muhammad, F., Zeng, L., Li, S., Huang, X., Jiao, B., Shiau Y., Li, D. 2019.
523 Solidification/stabilization of lead-zinc smelting slag in composite based geopolymer. J.
524 Clean Prod. 209, 1206-1215. https://doi.org/10.1016/j.jclepro.2018.10.265.
525 Xia, W. Y., Du, Y. J., Li, F. S., Li, C. P., Yan, X. L., Arulrajah, A., Wang, F., Song, D. J., 2019.
526 In-situ solidification/stabilization of heavy metals contaminated site soil using a dry jet
527 mixing method and new hydroxyapatite based binder. J. Hazard Mater. 369, 353-361.
528 https://doi.org/10.1016/j.jhazmat.2019.02.031.
529 Yin, J.H., 2001. Stress-strain-strength characteristics of soft Hong Kong marine deposits
530 without or with cement treatment. Lowl. Technol. Int.*3*(1), 1-13.
531 Yin, J.H., Fang, Z., 2006. Physical modelling of consolidation behaviour of a composite
532 foundation consisting of a cement-mixed soil column and untreated soft marine clay.
533 Geotechnique. *56*(1), 63-68. https://doi.org/10.1680/geot.2006.56.1.63.
534 Yin, J.H., and Fang, Z., 2010. Physical modeling of a footing on soft soil ground with deep
535 cement mixed soil columns under vertical loading. Mar. Georesour. Grotec. *28*(2), 173-188.
536 https://doi.org/10.1080/10641191003780872.
537 Yin, J.H., 2004. Properties and behaviour of a cement mixed Hong Kong marine clay and

538 design applications. Proceedings of a seminar on ground treatment. *Hong Kong, pp. 97-*
539 *105.*
540
541

Graphical Abstract

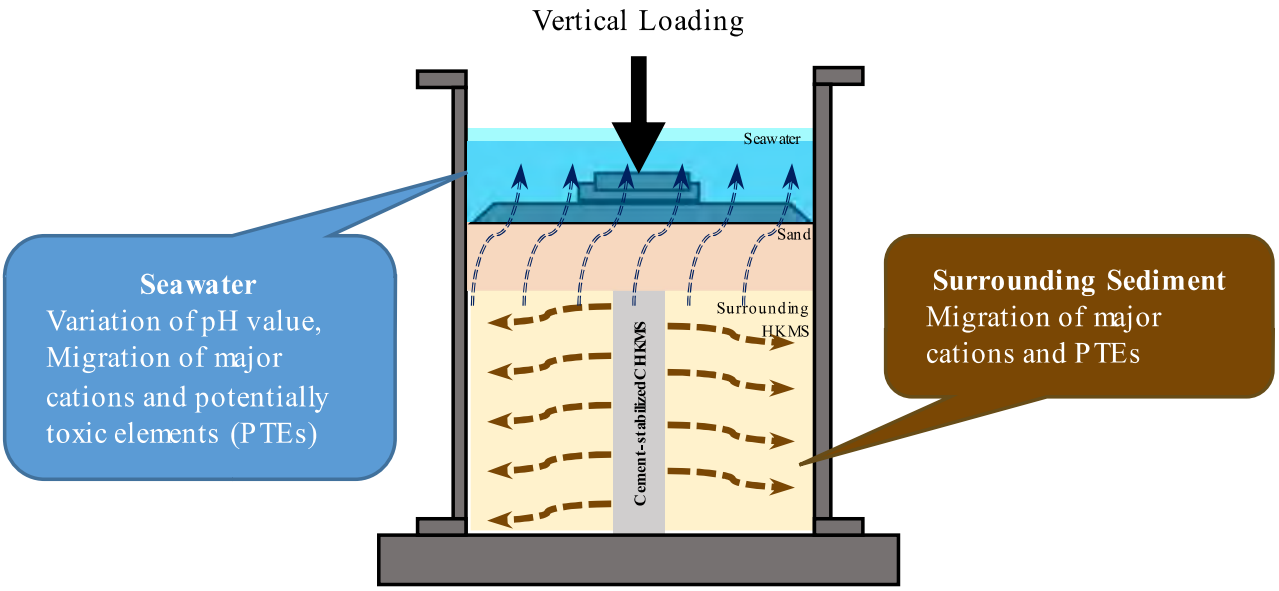

*Highlights (3 to 5 bullet points (maximum 85 characters including spaces per bullet point)

- Deep cement mixing (DCM) treatment of contaminated sediment was evaluated.
- Major cations were found to migrate into the seawater.
- Potentially toxic elements in the surrounding sediment remained stable.
- The risk of secondary pollution in the surrounding environment was low after DCM treatment.

List of Tables

Table 1. Physical properties of HKMS and CHKMS

	Specific Gravity	Liquid Limit (%)	Plastic Limit (%)	Plasticity Index (%)	pH Value	Loss of Ignition	Particle Size Distribution (%)		
							Sand	Silt	Clay
HKMS	2.65	53.5	27.4	26.1	7.72	4.33	5.5	65.5	29.0
CHKMS	2.60	59.3	27.5	31.8	7.11	4.31	3.5	77.5	19.0

Table 2. Total metal concentrations of HKMS and CHKMS

mg/kg	Cu	Zn	Cr	Ni	As
HKMS	16	71	36	21	6
CHKMS	15	87	38	23	9.5

Table 3. Chemical compositions of the cement binder

Components	SiO_2	Fe_2O_3	Al_2O_3	CaO	MgO	SO_3
Unit (%)	20.00	3.04	5.53	64.30	1.28	4.49

List of Figures

Supplementary Information

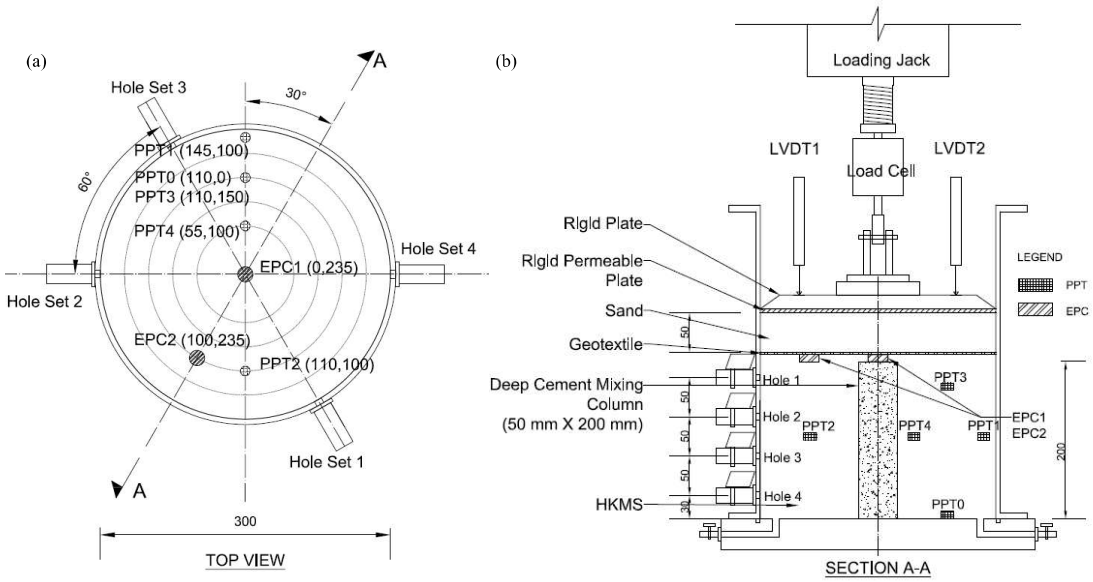

Fig. 1. Schematic diagram of the physical model (a) top view and (b) section view (dimensions in mm).

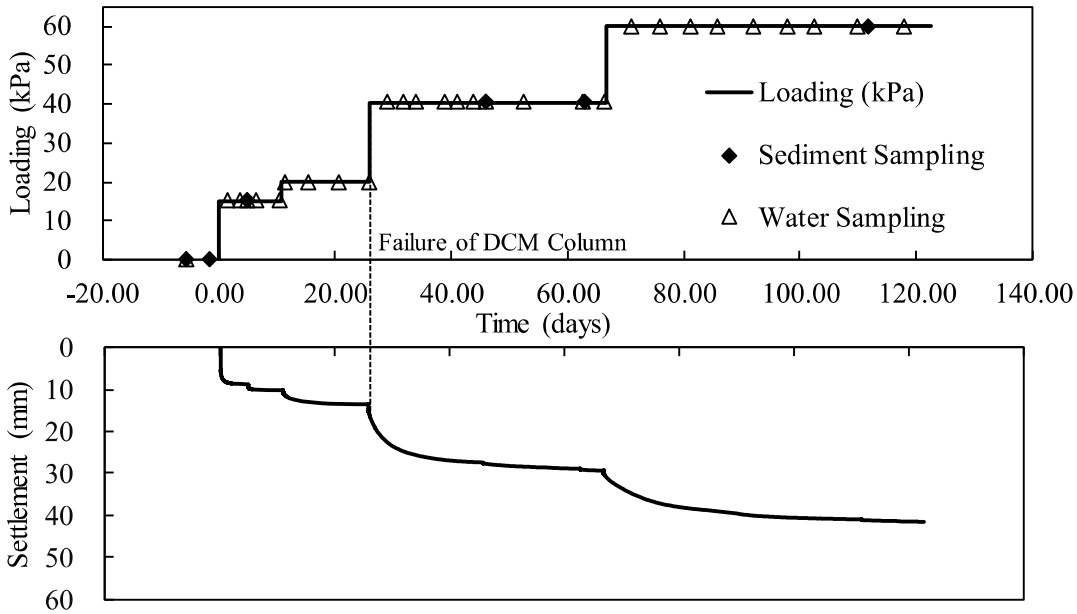

Fig. 2. Loading schedule and settlement with time.

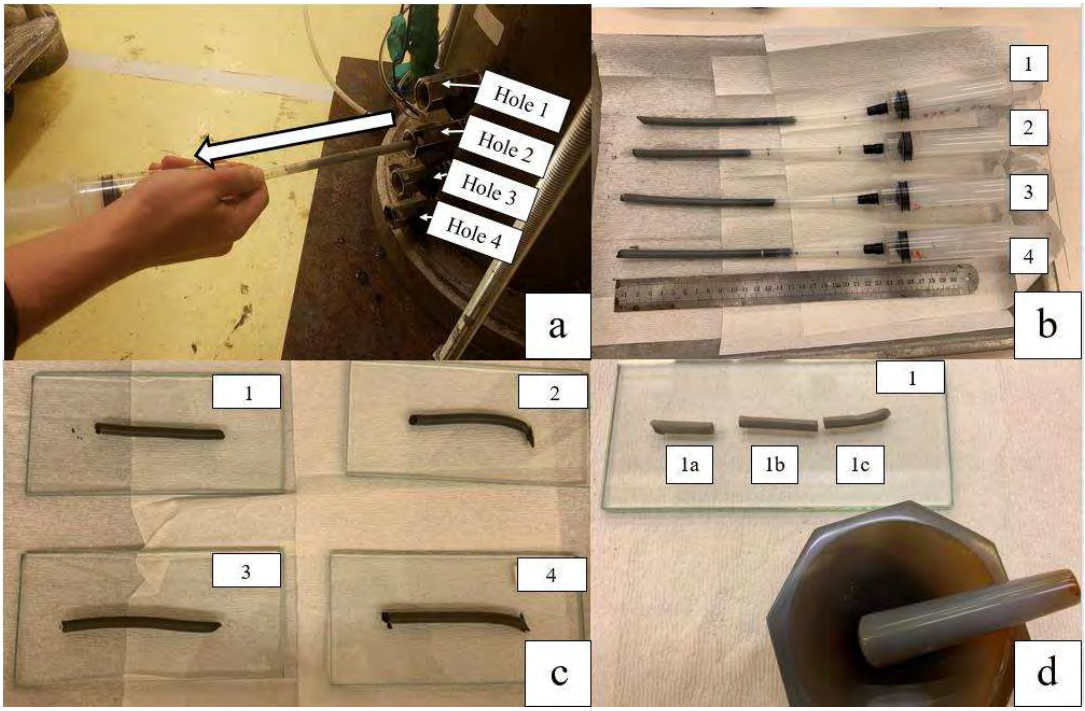

Fig. 3. Sediment sampling under 60 kPa loading: (a) from the model; (b) in sampling pipes, (c) on glass plates, and (d) in three sections for total digestion test.

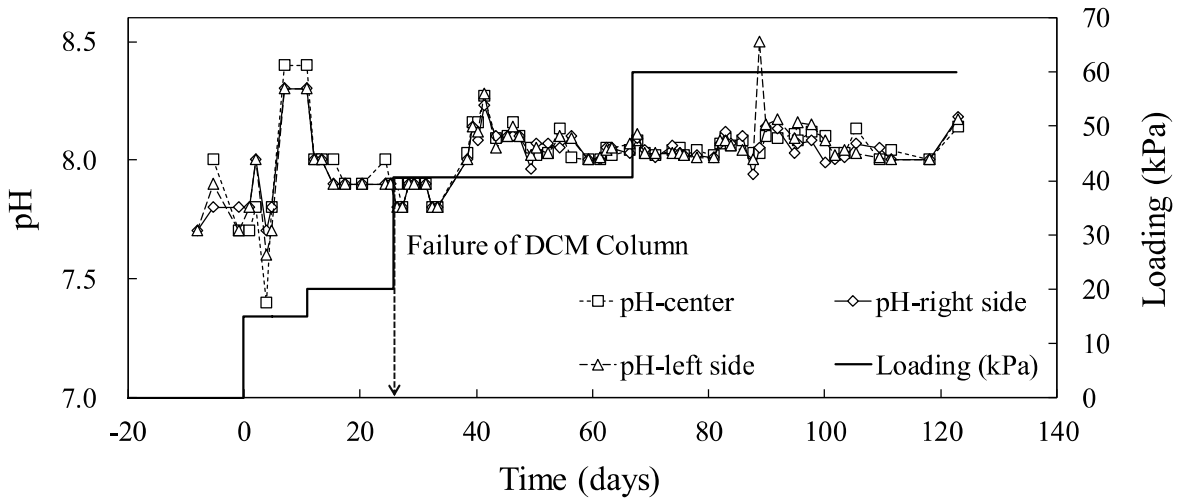

Fig. 4. The pH values of seawater *versus* time

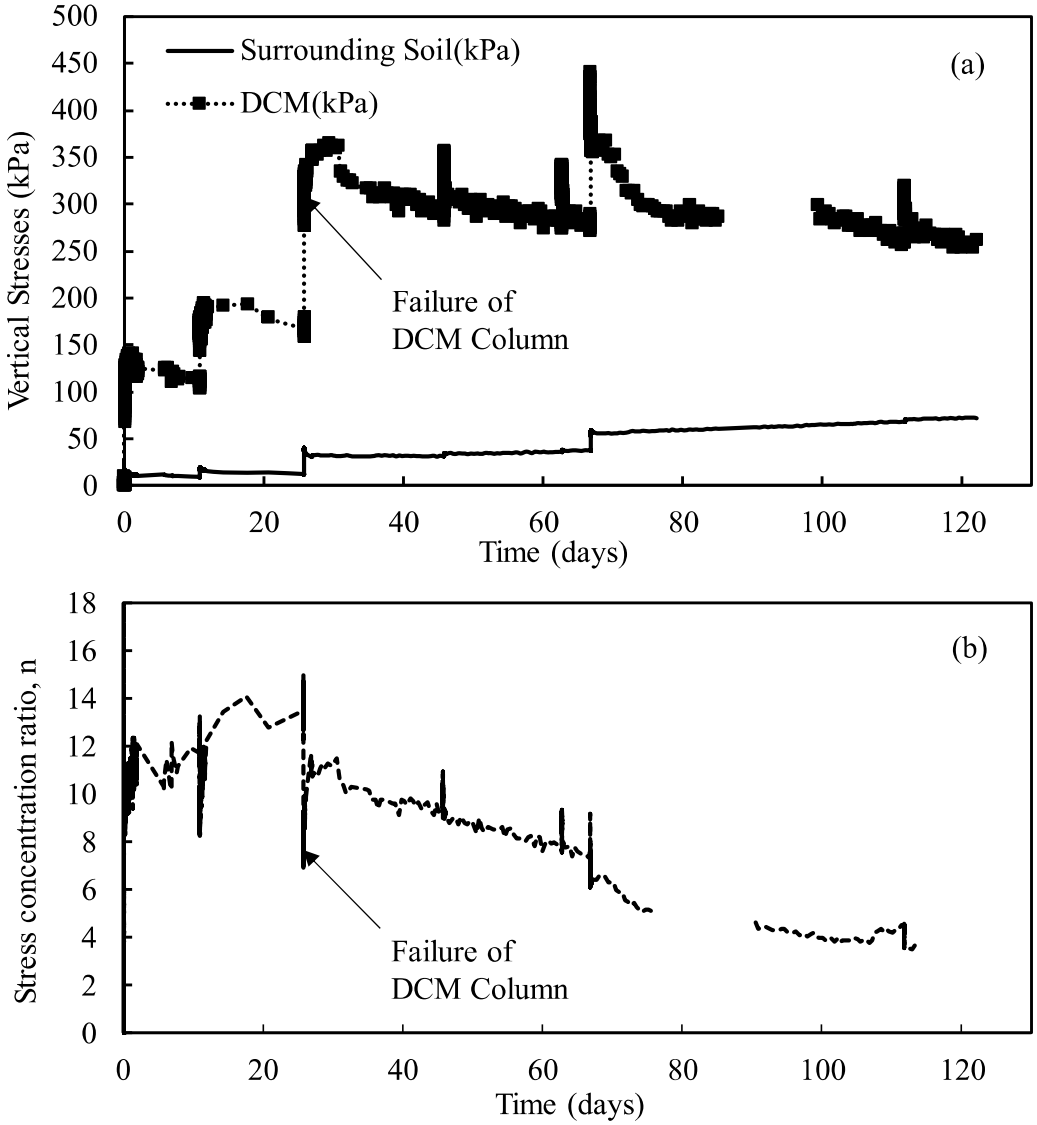

Fig. 5. (a) Vertical stresses on the DCM column and the surrounding sediment versus time and (b) the corresponding stress concentration ratio, n, versus time.

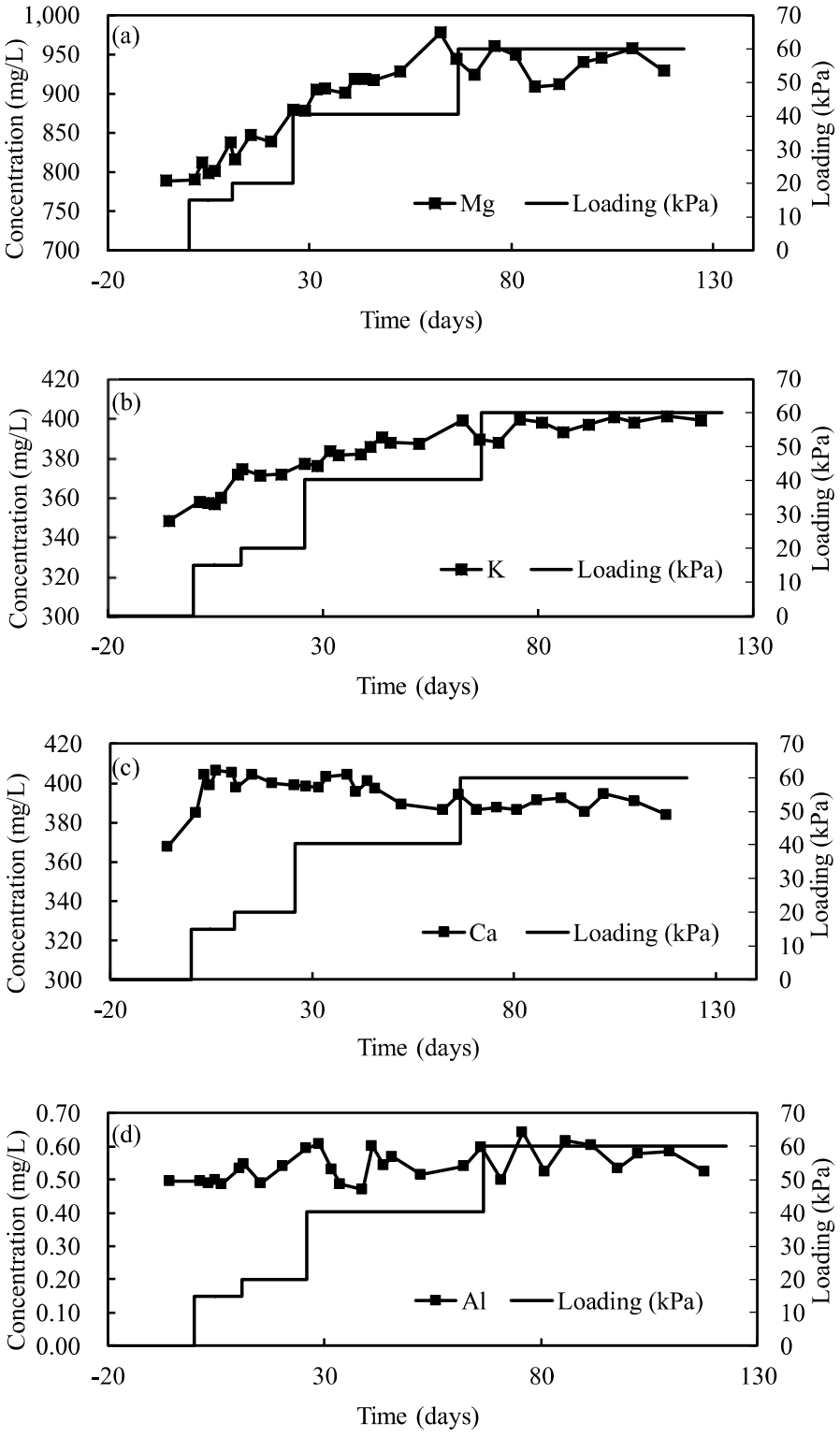

Fig. 6. Variation of major cation concentrations versus time with the corresponding loading schedule: (a) Mg; (b) Ca; (c) K; and (d) Al.

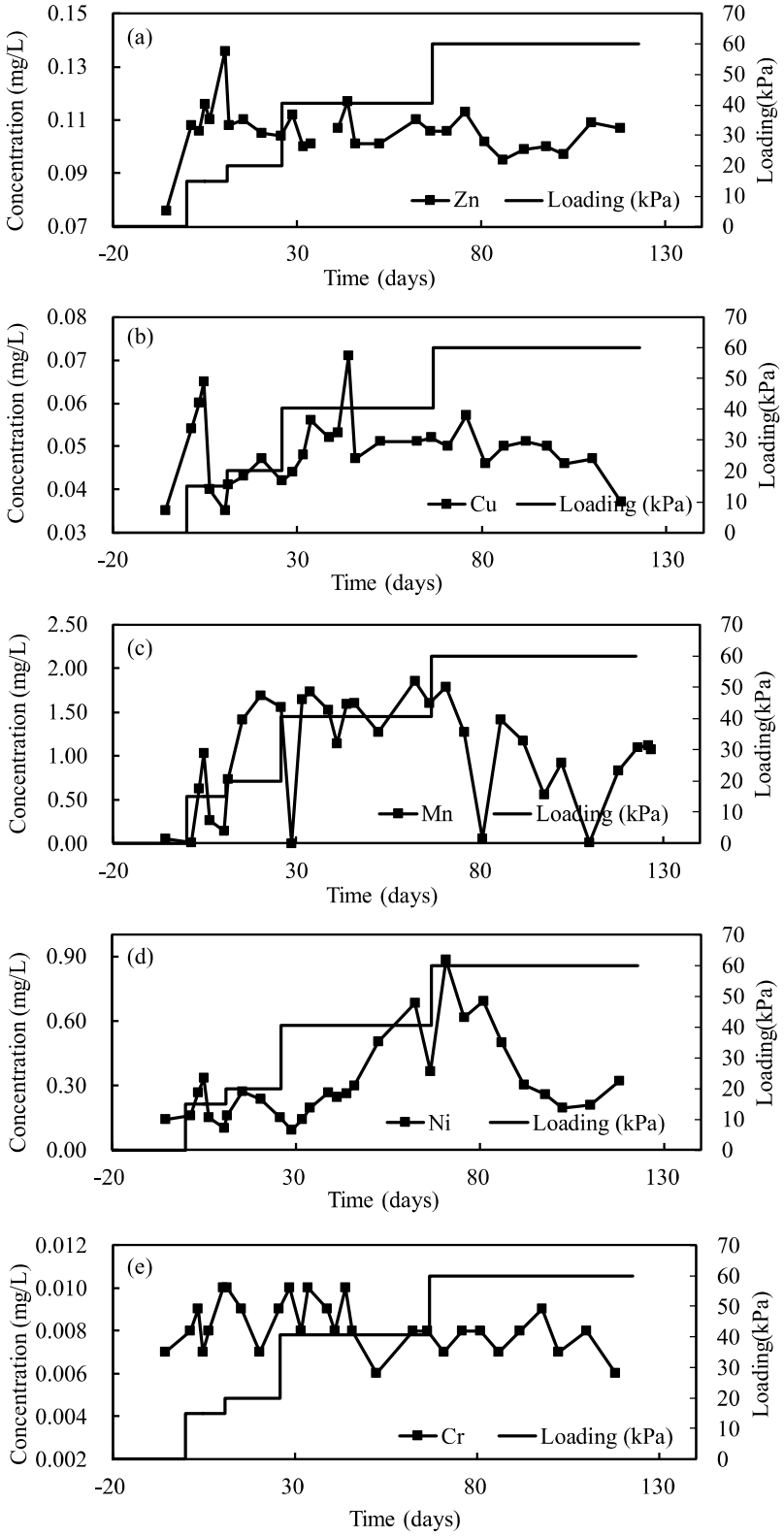

Fig. 7. Variation of PTEs concentrations versus time with the corresponding loading schedule: (a) Zn; (b) Cu; (c) Mn; (d) Ni and (e) Cr.

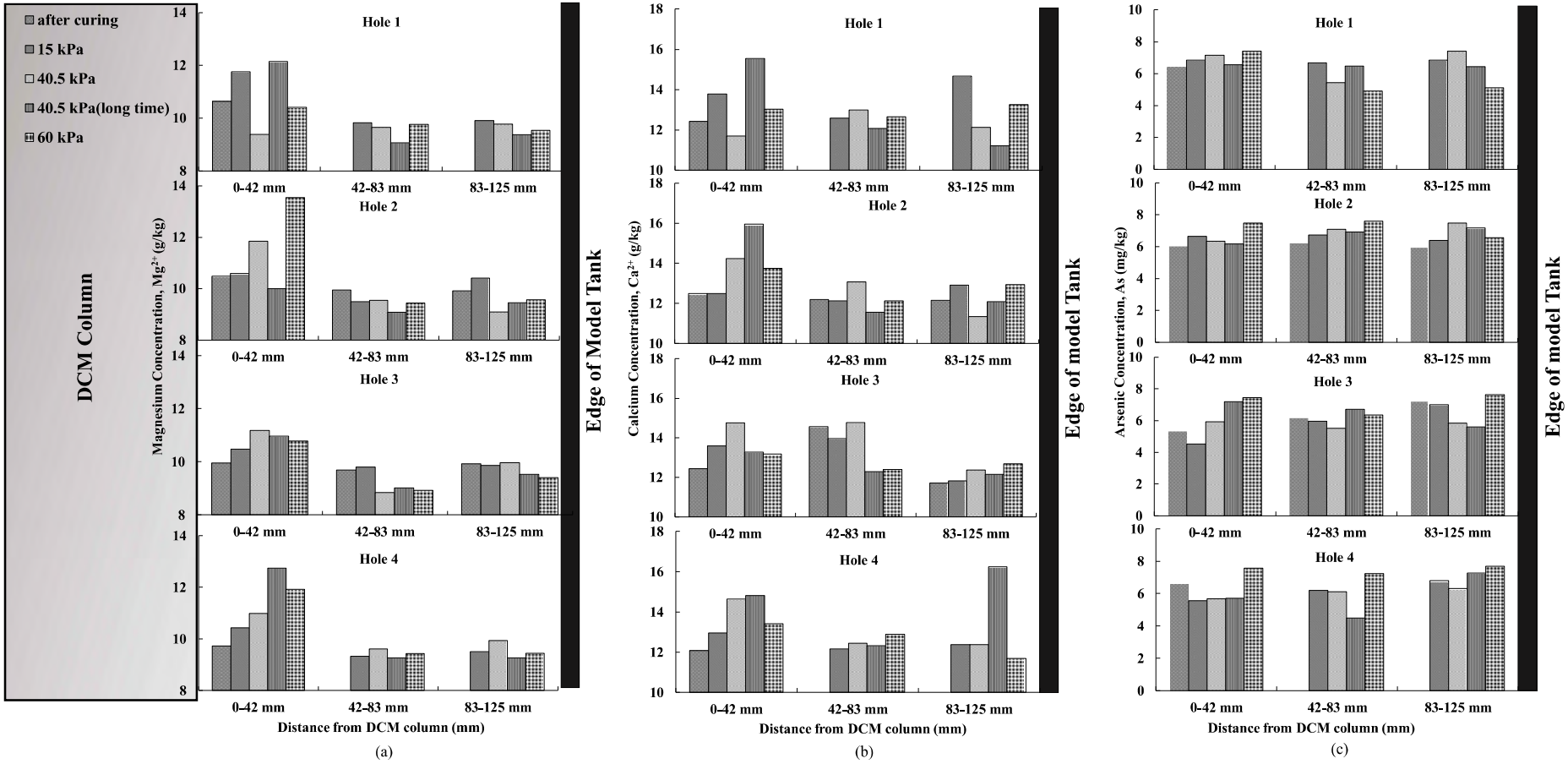

Fig. 8. Variation of (a) Mg, (b) Ca and (c) As concentrations at different locations in the surrounding sediment under different loadings.

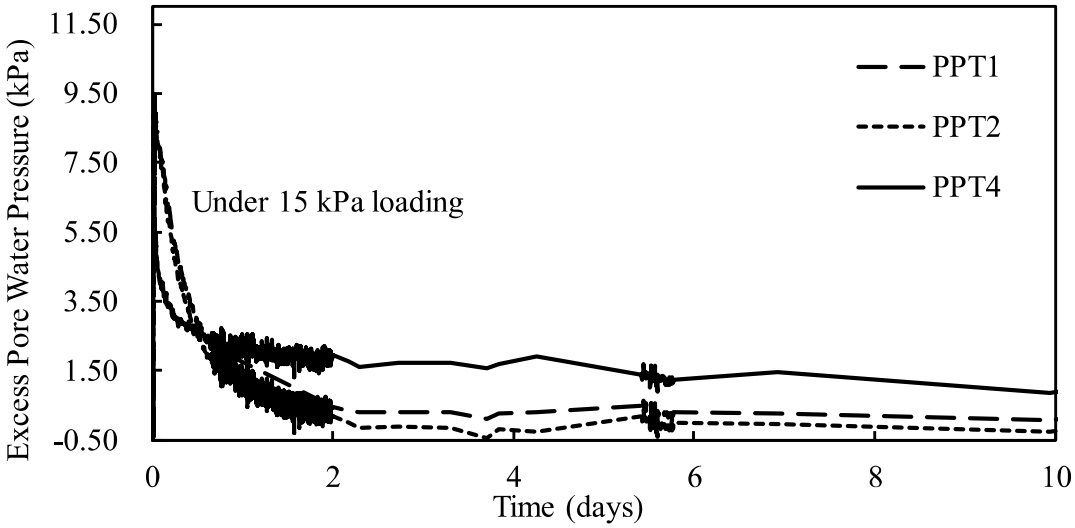

Fig. 9. Variation of excess pore water pressure versus time under 15 kPa of loading.

Supplementary Information

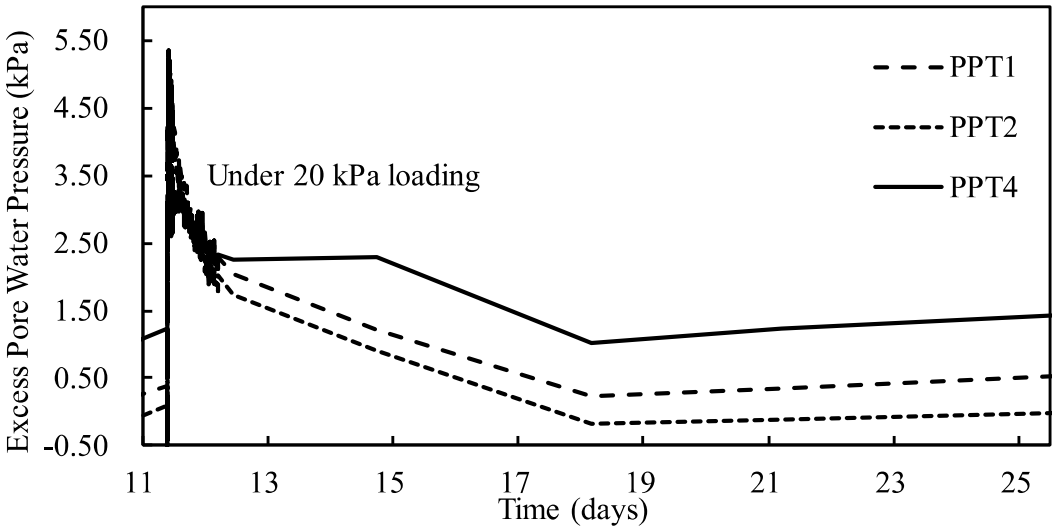

Fig. S1. Variation of excess pore water pressure *versus* time under 20 kPa of loading.

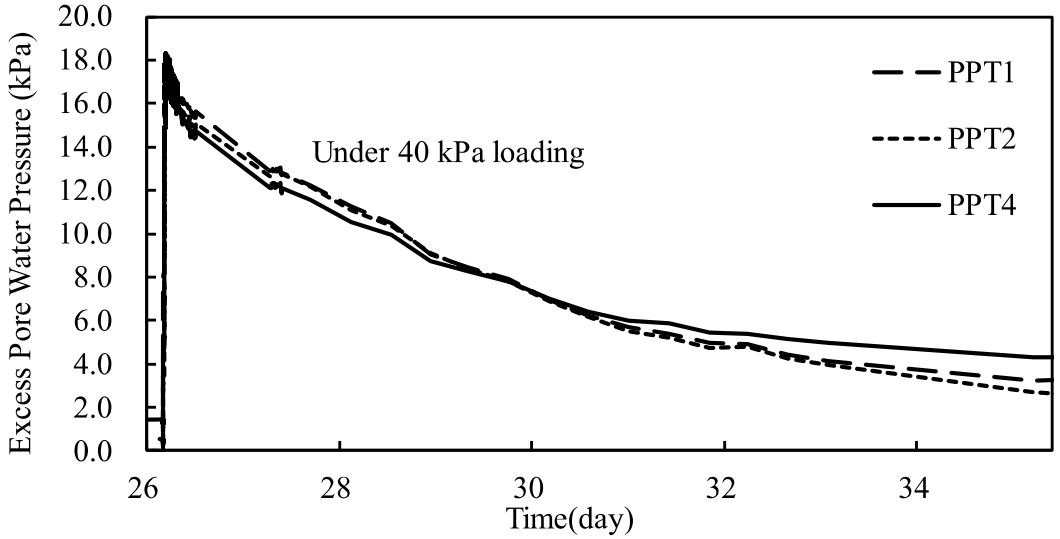

Fig. S2. Variation of excess pore water pressure *versus* time under 40 kPa of loading.

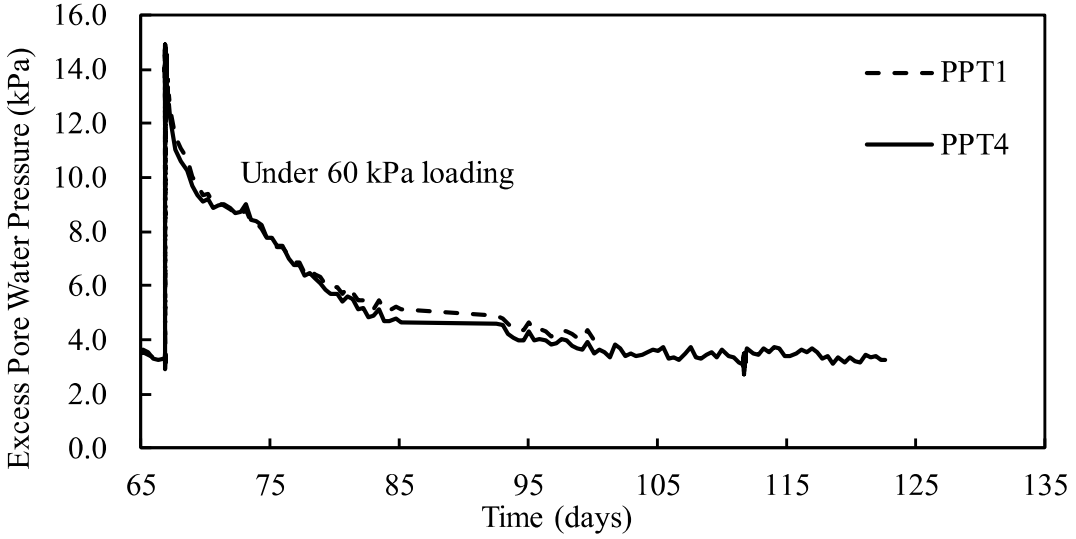

Fig. S3. Variation of excess pore water pressure *versus t*ime under 60 kPa of loading.